frontiers | Frontiers in Physics

TYPE Original Research
PUBLISHED 18 December 2025
DOI 10.3389/fphy.2025.1721662

1D-CNN for non-cooperative rotational Doppler signal extraction

Song Qiu[1]*, Jin Zheng[1], Yingjiao Shao[2], Minghui Xiong[1] and Qiang Wang[1]

[1]National Key Laboratory of Space Integrated Information System, Beijing, China, [2]Space Engineering University, Beijing, China

OPEN ACCESS

EDITED BY
Hao Jiang,
Huazhong University of Science and Technology, China

REVIEWED BY
Ravi Kumar Gangwar,
Indian Institute of Technology Dhanbad, India
Jia-Qi Lv,
Hebei University of Technology, China

*CORRESPONDENCE
Song Qiu,
qiusong20131111@126.com

RECEIVED 09 October 2025
REVISED 30 November 2025
ACCEPTED 03 December 2025
PUBLISHED 18 December 2025

CITATION
Qiu S, Zheng J, Shao Y, Xiong M and Wang Q (2025) 1D-CNN for non-cooperative rotational Doppler signal extraction. *Front. Phys.* 13:1721662.
doi: 10.3389/fphy.2025.1721662

The discovery of the rotational Doppler effect (RDE) has opened new opportunities for detecting parameters of rotating targets. In recent years, the physical mechanisms underlying this effect have been thoroughly investigated. However, existing methods for extracting target rotation rates remain largely confined to conventional spectral analysis techniques like Fourier transformation. In this study, we propose a machine learning-based approach for automatic rotation rate extraction, which enables rapid and accurate measurement under conditions which misalignment exists between vortex beam axis and the target rotating axis. This method significantly simplifies the rotation rate retrieval process while maintaining high precision. Furthermore, we provide an in-depth investigation into the intrinsic mechanisms of the algorithm, uncovering new physical insights that pave the way for practical applications of this technology.

KEYWORDS

CNN, convolutional neural network, machine learning (ML), measuremetn techniques, optical vortex, rotational Doppler effect (RDE), rotational speed

1 Introduction

The rotational Doppler effect (RDE) refers to the frequency shift in scattered light caused by relative motion between structured beams and rotating targets [1, 2]. Since the first demonstration by Padgett et al. in *Science* (2013) for rotational speed measurement [3], significant advancements have been made to enhance the practical applicability of this technique [4–9]. Initial implementations required strict alignment between the beam propagation axis and target rotation axis [10–12]. Subsequent studies extended this principle to misaligned configurations (non-cooperative detection), establishing new measurement methodologies under beam-target misalignment [13–15]. Recent progress has reduced the requirements for structured light characteristics: while early implementations demanded high-purity vortex beams, current approaches can utilize supercontinuum white light and even incoherent light sources [16, 17]. Notably, spectral broadening phenomena observed under both mode impurity and beam misalignment conditions exhibit frequency intervals matching rotational speeds. This discovery has led to the development of robust speed extraction methods based on spectral interval analysis [18–20], significantly expanding the technique's application potential.

Despite recent advancements in rotational speed detection based on the RDE, existing speed extraction methods university rely on spectral analysis of echo signals [21–25]. The conventional procedure involves: (1) acquiring time-domain echo signals, (2) performing frequency-domain analysis through Fourier transforms, (3) extracting spectral features, and (4) calculating rotational speeds. This approach suffers from computational complexity and dependence on expert interpretation, particularly under non-cooperative detection conditions where spectral signatures become highly intricate [26–28]. Manual analysis becomes impractical for accurate and efficient speed extraction in such scenarios. The rapid development of artificial intelligence technology has demonstrated remarkable capabilities across various domains [29]. Inspired by these advances, this study proposes an end-to-end deep learning model designed to directly regress rotational speeds from raw time-domain signals. This paradigm eliminates the need for frequency-domain conversion and manual feature engineering, thereby enhancing automation and computational efficiency.

Convolutional Neural Networks (CNNs) are a class of deep feedforward neural networks characterized by convolutional operations and hierarchical architectures, representing one of the cornerstone algorithms in deep learning [30–32]. Based on the CNN framework, this study proposes an end-to-end deep learning model based on one-dimensional convolutional neural network (1D-CNN), featuring a three-stage cascade structure composed of 1D convolutional and pooling players. This architecture enables progressive extraction of both local features and global temporal dependencies directly from raw time-domain signals. A full-process simulation of the RDE was implemented to generate a training dataset under non-cooperative detection conditions. Experimental validation demonstrates the model's superior predictive performance, achieving 90% accuracy in rotational speed estimation.

2 Theory

2.1 Non-cooperative rotational Doppler effect

The rotational Doppler effect (RDE) of vortex beams is well established, referring to the phenomenon where scattered light undergoes a frequency shift when orbital angular momentum (OAM) carrying structured beams illuminate a rotating object. The magnitude of this frequency shift depends on the structural parameters of the light beams and the rotational speed of the object. Consider the expression for a typical Laguerre–Gaussian (LG) mode vortex beam as Equation 1 [33]:

$$\mathrm{LG}_{p,l}(r,\varphi,z) = \frac{C}{\left(1+z^2/z_R^2\right)^{1/2}}\left(\frac{r\sqrt{2}}{w_z}\right)^{|l|} L_p^{|l|}\left(\frac{2r^2}{w_z^2}\right) \times \exp\left[-\frac{r^2}{w_z^2} + i\left(l\varphi - \frac{kr^2}{2R_z} - (2p+|l|+1)\arctan\frac{z}{z_R}\right)\right] \tag{1}$$

where p and l are the radial and azimuth index, respectively, C is a constant which stands for the amplitude, $L_p^{|l|}$ represents the generalized Laguerre polynomial of order p and degree $|l|$, z_R is the Rayleigh range expressed by $z_R = \pi w_0^2/\lambda$, where w_0 is the beam waist at the initial plane $(z = 0)$ where the beam is narrowest. The functions w_z, R_z are the beam waist and curvature radius of wavefront, respectively.

The Poynting vector refers to the energy flux density in an electromagnetic field, which can be expressed by $\vec{P} = \vec{E} \times \vec{B}$, where $\vec{E}$ represents the electric field intensity and $\vec{B}$ denotes the magnetic field intensity at a specific location. Based on the above LG expression, the Poynting vector within the vortex field can be expressed as,

$$\vec{P} = \frac{1}{c}\left[\frac{rz}{\left(z^2+z_R^2\right)}|u|^2\hat{r} + \frac{l}{kr}|u|^2\hat{\phi} + |u|^2\hat{z}\right] \tag{2}$$

where $\hat{r}$, $\hat{\phi}$ and $\hat{z}$ are unit vectors, $|u|^2 = |u(r,\varphi,z)|^2$ denotes the total energy intensity, and $k = 2\pi/\lambda$ denotes the wavenumber. It can be seen from Equation 2 that there are three independent component components in the Poynting vector, where the second term gives the skew angle of the Poynting vector with respect to the beam axis as,

$$\alpha = l/kr \tag{3}$$

For any scattering point under beam irradiation, when the scattering point moves along the direction of beam propagation (the direction of the Poynting vector) at a velocity v, the reflected light will experience a Doppler shift of $\Delta f = fv/c$, where f represents the frequency of the light. However, when the direction of motion does not coincide with the beam propagation axis, the calculation of the Doppler shift magnitude requires projecting the velocity of the scattering point onto the direction of beam propagation. For vortex beams, the Doppler shift for each scattering point within the irradiation range can be expressed as follows:

$$\Delta f = \frac{fv}{c} = \frac{2\omega R}{\lambda}\cdot \sin\alpha \tag{4}$$

Combining Equations 3, 4, the Doppler shift magnitude for each point is calculated to be $\Delta f = \ell\omega R/2\pi r$, where R represents the radius of the small scatter on the rotating object, while r denotes the beam radius at the scattering point. It can be seen that the magnitude of the Doppler shift generated at each point depends on its radial position (R) and the beam radius at that location. When the vortex beam illuminating the rotating object on its axis, for each scatterer, the beam radius always equals the scatterer rotating axis. Therefore, the Doppler shift becomes $\Delta f_{RDE} = \ell\omega/2\pi$, which is the so-called rotational Doppler shift. However, when the beam axis does not coincide with the object's axis of rotation (which can be called non-cooperative detection), the magnitude of the Doppler shift could relate with the position of each scatterer is not a uniform value. This is the fundamental principle of the non-cooperative rotational Doppler effect. At this point, it is no longer possible to directly calculate the target's rotational speed from the spectrum, as there is no single peak in the spectral.

2.2 1D-CNN model

This study proposes an end-to-end deep learning model based on 1D-CNN architecture to address the direct regression of target values from time-domain signals. Unlike conventional approached relying on Fourier transforms and manual feature computation, our model automatically learns frequency-domain latent features through multi-layer convolutional operations, eliminating intricate manual processing. The architecture accepts raw time-domain signals of length 1,002 as input and outputs target rotating speed information, with core design comprising two key components.

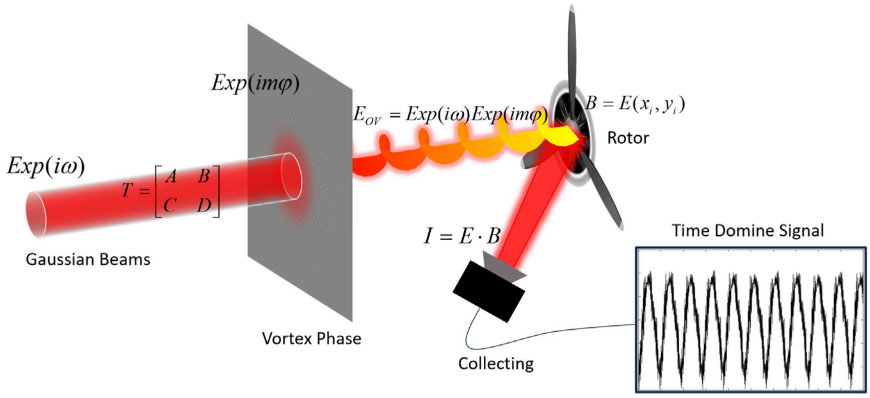

FIGURE 1
RDE simulation process. First, a Gaussian beam propagates through space according to the beam propagation matrix, subsequently interacting with a designed spiral phase mask of a vortex beam through multiplicative phase modulation to form a Laguerre–Gaussian vortex beam. Next, the generated vortex beam interacts with a rotating object characterized by a specific amplitude intensity distribution $B(x_i, y_i)$. The resulting scattered light is then fully captured based on the light intensity calculation formula. Finally, the collected signals are sampled to form time-domain signal data.

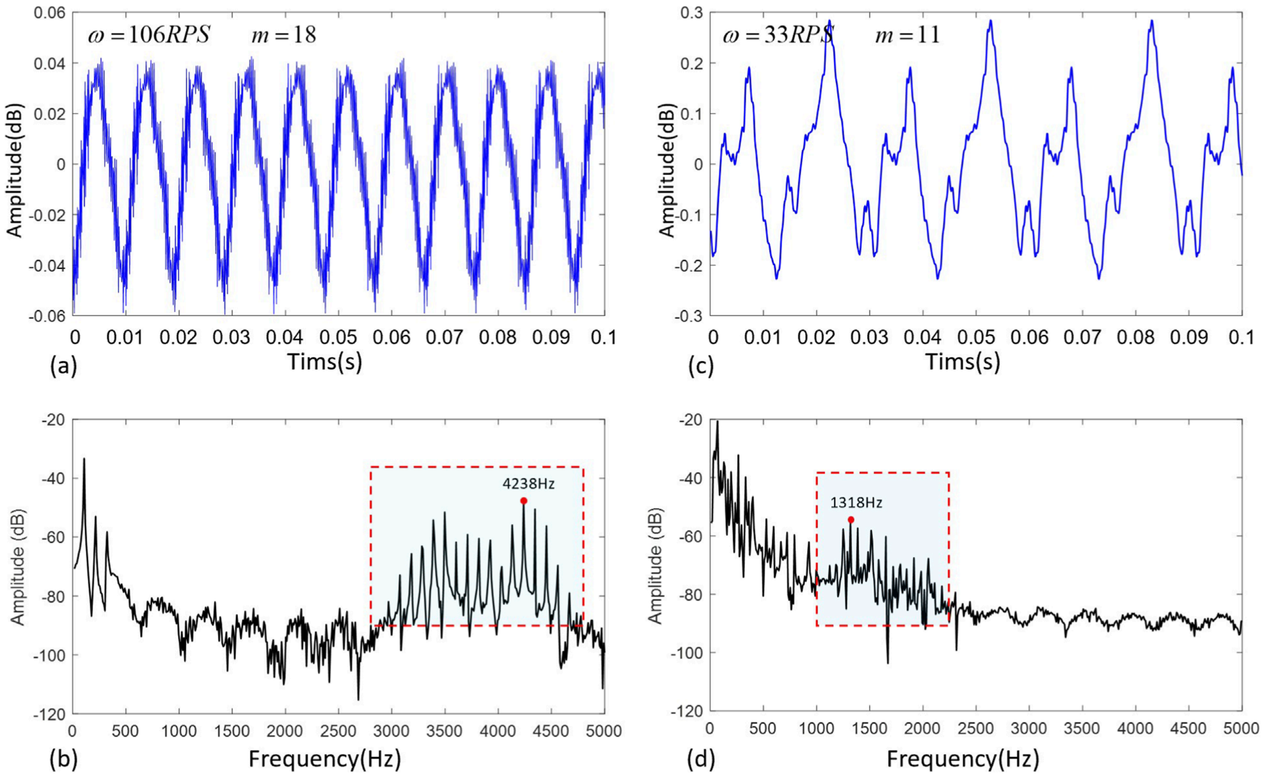

FIGURE 2
Time and Frequency domain signal of RDE. **(a,c)** represent the signals in the time domain, while **(b,d)** are the frequency domain signals. Under off-axis conditions, the frequency signals from both measurements shifted and exhibited broadening.

2.2.1 Feature extraction module

The architecture employs a three-stage cascade 1D convolutional-pooling hierarchy that hierarchically extracts both localized features and global patterns from time domain signals. Each stage progressively deploys 64, 128, and 256 filters (kernel size = 3), with ReLU activation introducing non-linearity and batch normalization (BN) accelerating convergence. Max-pooling (pooling size = 2), subsequently reduces feature dimensionality while enhancing robustness against minor temporal shifts in signals.

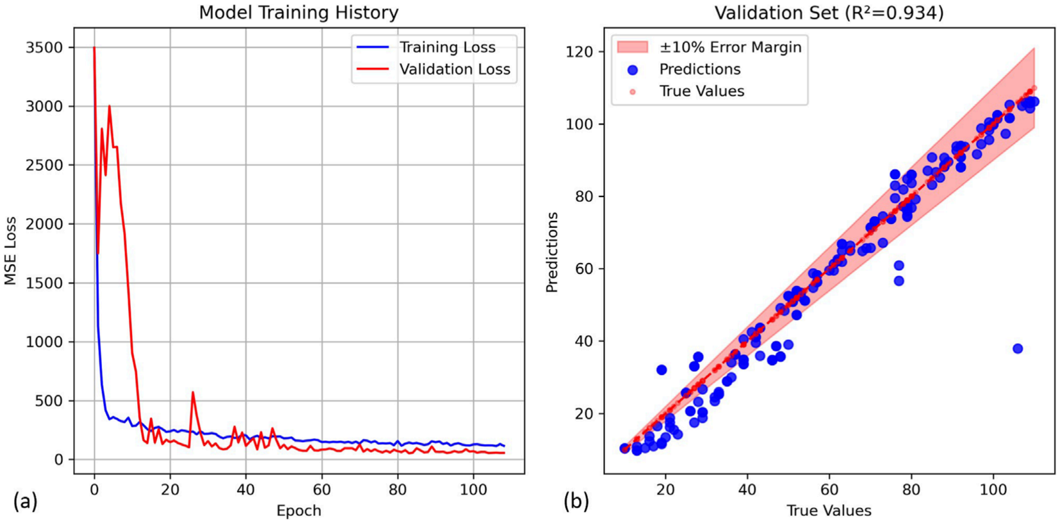

FIGURE 3
Training process and the predicted value. **(a)** The model training process with the decrease of MSE loss. **(b)** The predictions of the training sets with 10% error margin.

2.2.2 Feature compression and regression module

This module employs a structure incorporating global average pooling and fully-connected layers to achieve feature dimensionality reduction and value regression. The compressed feature tensor is projected into the target space through sequential operations. Firstly, global average pooling eliminates spatial redundancy while preserving discriminative patterns. Secondly, three dense layers (512->256->1 neurons) with dropout regularization (p = 0) prevent overfitting. And finally, adaptive SELU activation enables self-normalized propagation, ensuring stable gradient flow during end-to-end optimization.

2.2.3 Training strategy

The training strategy incorporated three technical components. Data preprocessing implemented cross-sample standardization on time-domain signals based on Equation 5.

$$X_{norm}(i) = \frac{X(i) - \mu_{time}}{\sigma_{time}} \tag{5}$$

where $X(i)$ denotes the raw signal value at the ith timestep, μ_{time} represents the mean value across all samples at the same timestep, and σ_{time} indicates the corresponding standard deviation. This operation eliminated dimensional inconsistencies while retaining temporal correlations.

For optimization, the mean squared error (MSE) loss function was employed to quantify prediction errors, with the Adam optimizer dynamically adjusting parameter update steps (initial learning rate: 1×10^{-3}) to balance convergence speed and stability. To control model complexity, and early stopping mechanism tracked validation loss trends, automatically halting training if no improvement persisted for 20 consecutive epochs, thereby preventing overfitting and ensuring generalizability to unseen non-cooperative detection scenarios.

3 Experiment

3.1 Design of the prove-of-concept experiment

To validate the feasibility of the aforementioned model, a comprehensive training dataset was first constructed in a simulated environment. Analogous to practical scenarios, the simulated data is generated through procedures including beam generation, diffraction propagation, illumination of rotating targets, scattered light collection, and sampling recording. As illustrated in Figure 1, a laser first generates Gaussian beam and then is converted into a vortex beam via a spiral phase $Exp(im\varphi)$, then interacts with the rotating target characterized by a specific amplitude intensity distribution, and finally generates time-domain signals through scattered light collection. More details of the simulation process can be found in Ref. [19].

When configuring the simulation parameters, the topological charge m of the vortex beam was set as a random integer between 10 and 25. Based on this value m, a superposition-state vortex beam was subsequently generated. The diffraction propagation distance was set to approximately 1 m. The rotational speed of the target was assigned a random value within the range of 10–110, consistent with the rotational speeds of common objects in daily life, such as fans and turbines. Regarding the parameters for off-axis illumination, the distance between the beam and the target's rotation center was set between 0 and r, where r denotes the radius of the vortex beam ring projected on the object's surface. The tilt angle between the beam propagations axis and the target's rotation axis was configured between 0 and $\pi/3$. Through the configuration of these parameters, realistic detection scenarios involving off-axis illumination of the target can be effectively simulated.

Based on the simulation parameter configuration, each set of training data includes: the target value, i.e., the preset rotational

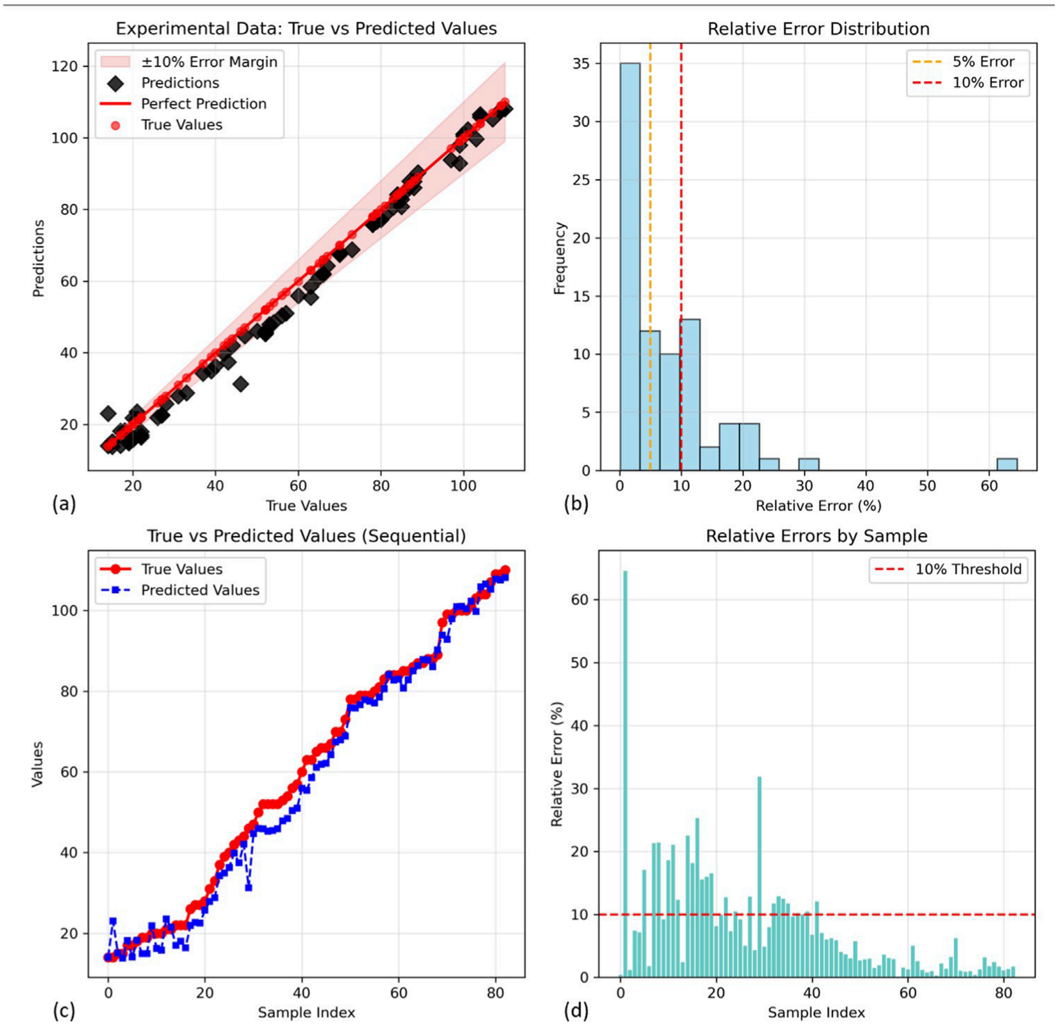

FIGURE 4
Prediction results of experimental data. **(a,b)** display the data ordered by the actual rotational speed values and the corresponding relative errors, respectively. This arrangement reveals that larger errors predominantly occur in the lower target speed range. In contract, **(c,d)** present the prediction outcomes and relative errors sorted by the index number of the experimental data. As evidenced, the majority of the experimental data demonstrate high prediction accuracy.

speed of the object, off-axis parameters, comprising lateral displacement and title angle, the topological charge *m* of the beam, the system sampling rate *f*, and the time-domain signal values obtained from sampling. To clearly illustrate the information contained in the training dataset, a sampled signal was selected and subjected to Fast Fourier Transform (FFT), with the results presented in Figure 2. We selected two sets of experimental data for time-frequency analysis. In the first dataset, as shown in Figures 2a, b, the rotational speed was set to 106 rounds per second (RPS), and the detection was performed using vortex beams with topological charges of ±18. Under ideal coaxial conditions where the beam propagation axis aligns with the target's rotation axis, the theoretical rotational Doppler shift would be 3,816 Hz. However, under off-axis illumination conditions, the signal deviated from its theoretical position and exhibited spectral broadening, with the highest peak observed at 4,238 Hz, as is shown in Figure 2b, making it impossible to accurately determine the target rotational speed. For the second dataset, as shown in Figures 2c, d, the rotational speed was set to 33 RPS, with probe beams carrying topological charges of ±11. Similarly, the signals displayed equally spaced broadening, preventing accurate calculate of the target rotational speed.

Subsequently, signal extraction experiments were conducted using our constructed 1D-CNN model. Based on the simulated rotational Doppler effect model, a total of 1,000 samples were collected to form the training dataset. During the 1D-CNN model training, the entire dataset was divided into training and test sets in an 8:2 ratio. In the initial training session, data containing all parameters were used as training inputs to train the model, and the results are illustrated in Figure 3. Here, Figure 3a represents the descent process of the training loss, while Figure 3b is the prediction results of the validation set. It can be observed from the training history that the loss decreased to an acceptable range after approximately 110 training epochs, at which point the model ceased training. In the validation datasets, the predicted

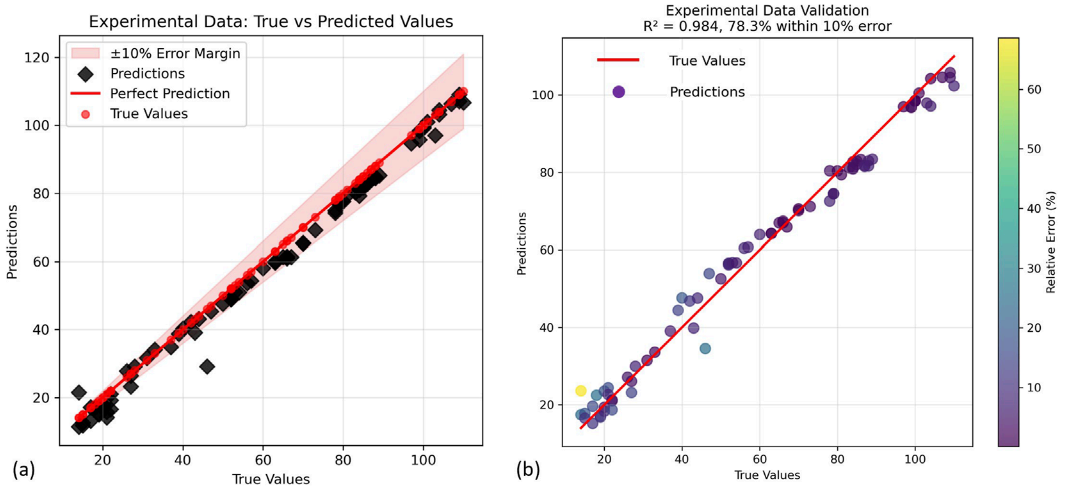

FIGURE 5
Prediction results without beam displacement parameters **(a)** and probe beam topological charge **(b)** information. The results demonstrate that the model maintains high predictive accuracy in such condition. This indicates that the implemented algorism deduces rotational speed by learning characteristic patterns in the spectral distribution of the experimental data.

values generally align closely with the true values. The prediction errors for most datasets remain 10%, with the exception of a few outliers. Furthermore, the model demonstrates higher prediction accuracy when the target rotational speed ranges between 30 and 100 RPS, whereas its performance degrades significantly at speeds below 25 RPS.

3.2 Key parameter analysis

Based on the pre-trained model mentioned above, we first evaluated its performance using experimental data with all parameters intact. The rotational speed in the experimental data was set to random values between 1 and 100 RPS while the topological charge was configured between 15 and 30. Each dataset included parameters such as lateral displacement, tilt angle, sampling rate, the topological charge of the probe beam, and complete time-frequency signals. The prediction results of the model are shown in Figure 4. It can be observed that under the condition of complete parameters, the model effectively extracts the target rotational speed embedded in the measurement data. Across a total of 83 experimental datasets, the maximum prediction error observed was 64.5%, where the true rotational speed of the target is 14 RPS while the predicted value reached 23.04 RPS. In contrast, the optimal prediction was achieved with dataset 58, recording a true value of 84 RPS against a predicted value of 84.11 RPS, resulting in a negligible error of merely 0.1%. Over 70% of the datasets exhibited relative prediction errors within 10%, demonstrating the model's strong predictive capability.

Based on the aforementioned analysis and experimental procedures, the prediction results demonstrate that the model has acquired the capability to compute the target's rotational speed by integrating time-domain signals with relevant detection and sampling parameters. However, these experimental outcomes alone cannot fully reveal the model's decision-making mechanism. To further determine whether the 1D-CNN learned the underlying Doppler effect principles or merely identified patterns in the frequency spectrum, we conducted an additional test by omitting the beam displacement parameters and the vortex beam topological charge. To maintain consistent input dimensions for the model, the omitted parameters were replaced with zeros. The results of this test are presented in Figure 5.

As shown in the prediction results, the model continues to accurately predict the target rotational speed with minimal error. The maximum prediction error reached 68.6% (only 1 set), while 78.3% of predictions maintained errors within 10%, demonstrating that the model's predictive accuracy remains unaffected by the omission of beam displacement and probe beam parameters. In contrast, traditional frequency analysis methods are difficult to precisely calculate the rotational speed from spectral information when accurate beam topological charge parameters omitted, the model successfully extracted the rotational speed. This indicates that the model deduces the rotational speed based on characteristic features in the frequency signal, rather than relying on the conventional rotational Doppler effect principle.

4 Conclusion and discussion

In summary, to address the challenge of extracting rotational speed information from broadened rotational Doppler shift signals under non-cooperative conditions, this paper proposes an adaptive target rotational speed extraction method based on a machine learning model. A one-dimensional convolutional neural network (1D-CNN) was developed, and through optimized architecture design, the model successfully achieves accurate extraction of target rotational speed under off-axis illumination conditions. Based on the established RDE simulation process, a training dataset was constructed under off-axis illumination conditions, and the model was trained to its optimal state. The trained model was subsequently applied to predict experimental data, with results indicating high accuracy for most predictions and an overall error within 10%, demonstrating the model's robust predictive performance. However, the current training data does not account for environment noise such as atmosphere turbulence. Subsequent studies could further enhance the model's robustness by diversifying the training dataset.

Comparative experiments further verified that the algorithm can extract the target rotational speed solely from the frequency information inherent in the spectrum, without requiring beam displacement or vortex beam parameters, thereby significantly improving the efficiency the speed extraction. The proposed model effectively solves the problem of extracting target rotational speed under off-axis vortex beam illumination, advancing the practical application of RDE-based methods from theoretical research to real-world implementation.

Data availability statement

The raw data supporting the conclusions of this article will be made available by the authors, without undue reservation.

Author contributions

SQ: Methodology, Writing – review and editing, Data curation, Writing – original draft. JZ: Validation, Supervision, Writing – original draft. YS: Writing – review and editing, Validation. MX: Writing – review and editing, Investigation, Formal Analysis. QW: Project administration, Resources, Writing – review and editing.

Funding

The author(s) declared that financial support was received for this work and/or its publication. This work was partly supported by the National Natural Science Foundation of China under grant 62305007 and partly supported by the Internal Funding of National Key Laboratory of Space Integrated Information System.

Conflict of interest

The author(s) declared that this work was conducted in the absence of any commercial or financial relationships that could be construed as a potential conflict of interest.

Generative AI statement

The author(s) declared that generative AI was not used in the creation of this manuscript.

Any alternative text (alt text) provided alongside figures in this article has been generated by Frontiers with the support of artificial intelligence and reasonable efforts have been made to ensure accuracy, including review by the authors wherever possible. If you identify any issues, please contact us.

Publisher's note

References

1. Garetz BA. Angular doppler effect. *J Opt Soc Am B* (1981) 71:609–11. doi:10.1364/josa.71.000609

2. Bialynicki-Birula I, Bialynicka-Birula Z. Rotational frequency shift. *Phys Rev Lett* (1997) 78:2539–42. doi:10.1103/physrevlett.78.2539

3. Lavery MP, Speirits FC, Barnett SM, Padgett MJ. Detection of a spinning object using light's orbital angular momentum. *Science* (2013) 341:537–40. doi:10.1126/science.1239936

4. Korech O, Steinitz U, Gordon RJ, Averbukh IS, Prior Y. Observing molecular spinning via the rotational doppler effect. *Nat Photon* (2013) 7:711–14. doi:10.1038/nphoton.2013.189

5. Fu S, Wang T, Zhang Z, Zhai Y, Gao C. Non-diffractive bessel-gauss beams for the detection of rotating object free of obstructions. *Opt Express* (2017) 25:20098–108. doi:10.1364/OE.25.020098

6. Kang L, Cheng Y, Xiang L, Wang H, Qin Y, Yue G. Spinning target detection using OAM-Based radar. In: International Workshop on Electromagnetics: Applications and Student Innovation Competition; 30 May 2017 - 01 June 2017; London, UK. IEEE (2017). p. 29–30.

7. Fang L, Padgett MJ, Wang J. Sharing a common origin between the rotational and linear doppler effects. *Laser Photon Rev.* (2017) 11:1700183. doi:10.1002/lpor.201700183

8. Deng J, Li KF, Liu W, Li G. Cascaded rotational doppler effect. *Opt Lett* (2019) 44:2346–49. doi:10.1364/OL.44.002346

9. Anderson AQ, Strong EF, Heffernan BM, Siemens ME, Rieker GB, Gopinath JT. Detection technique effect on rotational doppler measurements. *Opt Lett* (2020) 45:2636–9. doi:10.1364/OL.390425

10. Rosales-Guzman C, Hermosa N, Belmonte A, Torres JP. Direction-sensitive transverse velocity measurement by phase-modulated structured light beams. *Opt Lett* (2014) 39:5415–10. doi:10.1364/OL.39.005415

11. Zhou H, Fu D, Dong J, Zhang P, Zhang X. Theoretical analysis and experimental verification on optical rotational doppler effect. *Opt Express* (2016) 24:10050–6. doi:10.1364/OE.24.010050

12. Hu XB, Zhao B, Zhu ZH, Gao W, Rosales-Guzman C. *In situ* detection of a cooperative target's longitudinal and angular speed using structured light. *Opt Lett* (2019) 44:3070–3. doi:10.1364/OL.44.003070

13. Qiu S, Liu T, Li Z, Wang C, Ren Y, Shao Q. Influence of lateral misalignment on the optical rotational doppler effect. *Appl Opt* (2019) 58:2650–5. doi:10.1364/AO.58.002650

14. Qiu S, Liu T, Ren Y, Li Z, Wang C, Shao Q. Detection of spinning objects at oblique light incidence using the optical rotational doppler effect. *Opt Express* (2019) 27:24781–92. doi:10.1364/OE.27.024781

15. Lü J-Q, Cheng T-Y, Guo J-X, Li J-S, Wang Y, Lu Z. Robust measurement of angular velocity based on rotational doppler effect in misaligned illumination. *Appl Phys Lett* (2023) 123:131107. doi:10.1063/5.0163937

16. Lavery MPJ, Barnett SM, Speirits FC, Padgett MJ. Observation of the rotational doppler shift of a white-light, orbital-angular-momentum-carrying beam backscattered from a rotating body. *Optica* (2014) 1:1–4. doi:10.1364/optica.1.000001

17. Zhao X, Lu X, Hu Z, Liu T, Hang Y, Gao J. Robust detection of a rotational doppler shift with randomly fluctuated light. *Opt Lett* (2024) 49:4198–201. doi:10.1364/OL.524332

18. Qiu S, Ding Y, Liu T, Liu Z, Ren Y. Rotational object detection at noncoaxial light incidence based on the rotational doppler effect. *Opt Express* (2022) 30:20441–50. doi:10.1364/OE.461179

19. Qiu S, Ding Y, Liu T, Liu Z, Wu H, Ren Y. Fragmental optical vortex for the detection of rotating object based on the rotational doppler effect. *Opt Express* (2022) 30:47350–60. doi:10.1364/OE.476870

20. Qiu S, Liu T, Ding Y, Liu Z, Chen L, Ren Y. Rotational doppler effect with vortex beams: fundamental mechanism and technical progress. *Front Phys* (2022) 10:938593. doi:10.3389/fphy.2022.938593

21. Ren Y, Qiu S, Liu T, Liu Z. Compound motion detection based on OAM interferometry. *Nanophotonics* (2022) 11:1127–35. doi:10.1515/nanoph-2021-0622

22. Zhai Y, Fu S, Yin C, Zhou H, Gao C. Detection of angular acceleration based on optical rotational doppler effect. *Opt Express* (2019) 27:15518–27. doi:10.1364/OE.27.015518

23. Zhang W, Zhang D, Qiu X, Chen L. Quantum remote sensing of the angular rotation of structured objects. *Phys Rev A* (2019) 100:043832. doi:10.1103/physreva.100.043832

24. Qiu S, Ren Y, Liu T, Chen L, Wang C, Li Z. Spinning object detection based on perfect optical vortex. *Opt Lasers Eng* (2020) 124:105842. doi:10.1016/j.optlaseng.2019.105842

25. Zhai Y, Fu S, Zhang J, Lv Y, Zhou H, Gao C. Remote detection of a rotator based on rotational doppler effect. *Appl Phys Express* (2020) 13:022012. doi:10.35848/1882-0786/ab6e0c

26. Deng D, Zhao H, Ni J, Li Y, Qiu C-W. A phase-to-intensity strategy of angular velocity measurement based on photonic orbital angular momentum. *Nanophotonics* (2022) 11:865–72. doi:10.1515/nanoph-2021-0461

27. Emile O, Rochefort G, Le Stradic K, Emile J. Air vortex detection using the rotational doppler effect. *Appl Opt* (2024) 63:7669. doi:10.1364/ao.534245

28. Larnimaa S, Vainio M. Fourier-transform spectroscopy based on the rotational doppler effect. *AIP Adv* (2024) 14:105329. doi:10.1063/5.0220119

29. Wang H, Yang X, Liu Z, Pan J, Meng Y, Shi Z. Deep-learning-based recognition of multi-singularity structured light. *Nanophotonics* (2021) 0. doi:10.1515/nanoph-2021-0489

30. Sato T, Hotta K. CNN to capsule network transformation. In: 2020 Digital Image Computing: Techniques and Applications (DICTA); 29 November 2020 - 02 December 2020; Melbourne, Australia. IEEE (2020) 1–2.

31. Cheng WY, Wan ZW, Chen YD, Chen ZW. Automatic classification of ionogram with CNN. In: 2020 IEEE International Conference on Consumer Electronics - Taiwan (ICCE-Taiwan); 28-30 September 2020; Taoyuan, Taiwan. IEEE (2020) 1–2.

32. Tian C, Xu Y, Zuo W, Lin CW, Zhang D. Asymmetric CNN for image superresolution. *IEEE Trans Syst Man, Cybernetics* (2022) 52:3718–30. doi:10.1109/tsmc.2021.3069265

33. Allen L, Beijersbergen MW, Spreeuw RJ, Woerdman JP. Orbital angular momentum of light and the transformation of laguerre-gaussian laser modes. *Phys Rev A* (1992) 45:8185–9. doi:10.1103/physreva.45.8185